The SunCHECK™ Platform powers Quality Management in radiation therapy.

Scalable to meet the needs of any clinic or network, SunCHECK helps:

- **Reduce risks**
- **Control costs**
- **Improve treatment quality**

Visit sunnuclear.com to learn how SunCHECK fits into your clinic.

Patient Safety Starts Here

SUN NUCLEAR corporation

MEDICAL PHYSICS

Technical Note: A preliminary study of dual-tracer PET image reconstruction guided by FDG and/or MR kernels

Haiyan Wang[1,2] | Zhenxing Huang[1] | Qiyang Zhang[1] | Dongfang Gao[1] | Zhanglei OuYang[1] | Dong Liang[1,3] | Xin Liu[1,3] | Yongfeng Yang[1,3] | Hairong Zheng[1,3] | Zhanli Hu[1,3]

[1]Lauterbur Research Center for Biomedical Imaging, Shenzhen Institute of Advanced Technology, Chinese Academy of Sciences, Shenzhen, China

[2]Shenzhen College of Advanced Technology, University of Chinese Academy of Sciences, Beijing, China

[3]Chinese Academy of Sciences Key Laboratory of Health Informatics, Shenzhen, China

Correspondence
Zhanli Hu, Lauterbur Research Center for Biomedical Imaging, Shenzhen Institute of Advanced Technology, Chinese Academy of Sciences, Shenzhen, China.
Email: zl.hu@siat.ac.cn

Abstract

Purpose: Clinically, single radiotracer positron emission tomography (PET) imaging is a commonly used examination method; however, since each radioactive tracer reflects the information of only one kind of cell, it easily causes false negatives or false positives in disease diagnosis. Therefore, reasonably combining two or more radiotracers is recommended to improve the accuracy of diagnosis and the sensitivity and specificity of the disease when conditions permit.

Methods: This paper proposes incorporating ^{18}F-fluorodeoxyglucose (FDG) as a higher-quality PET image to guide the reconstruction of other lower-count ^{11}C-methionine (MET) PET datasets to compensate for the lower image quality by a popular kernel algorithm. Specifically, the FDG prior is needed to extract kernel features, and these features were used to build a kernel matrix using a k-nearest-neighbor (kNN) search for MET image reconstruction. We created a 2-D brain phantom to validate the proposed method by simulating sinogram data containing Poisson random noise and quantitatively compared the performance of the proposed FDG-guided kernelized expectation maximization (KEM) method with the performance of Gaussian and non-local means (NLM) smoothed maximum likelihood expectation maximization (MLEM), MR-guided KEM, and multi-guided-S KEM algorithms. Mismatch experiments between FDG/MR and MET data were also carried out to investigate the outcomes of possible clinical situations.

Results: In the simulation study, the proposed method outperformed the other algorithms by at least 3.11% in the signal-to-noise ratio (SNR) and 0.68% in the contrast recovery coefficient (CRC), and it reduced the mean absolute error (MAE) by 8.07%. Regarding the tumor in the reconstructed image, the proposed method contained more pathological information. Furthermore, the proposed method was still superior to the MR-guided KEM method in the mismatch experiments.

Conclusions: The proposed FDG-guided KEM algorithm can effectively utilize and compensate for the tissue metabolism information obtained from dual-tracer PET to maximize the advantages of PET imaging.

1 | INTRODUCTION

Positron emission tomography (PET) uses radionuclide-labeled biomolecules as tracers to detect biochemical, metabolic, and other functional changes in vivo.[1,2] PET has been widely used in the early diagnosis of tumors, cardiology, and neurological diseases and the development of highly promising new drugs; therefore, it is currently an outstanding representative of functional molecular imaging technology.[3-5]

In clinical practice, single-tracer PET imaging is a commonly used examination method; however, since each radioactive tracer can reflect the information of only one kind of cell, it can lead to false negatives or false positives in disease diagnosis. Therefore, if conditions permit, it is recommended to reasonably combine two or more radiotracers to improve the accuracy of diagnosis and characterization of the tumor and achieve better sensitivity and specificity. In some clinical cases and research experiments, PET imaging using multiple tracers has been employed to characterize various aspects of pathology.[6-8] For example, in the use of imaging for the grading of glioma, when ^{11}C-methionine (MET) flows into the body, it can participate in protein synthesis or be converted into S-adenosylmethionine as a methyl donor, so it can reflect amino acid transport metabolism and protein synthesis in the living body.[10,11] Moreover, due to the low counts of the background, the MET tumor imaging has better tissue contrast, but there is still a certain overlap between high-grade and low-grade glioma.[9] The imaging principle of ^{18}F-fluorodeoxyglucose (FDG) is that the metabolism of tumor cells in malignant tumor tissues is enhanced and cell proliferation is accelerated, so that the expression of glucose transporter mRNA increases and the level of the glucose transporter improves accordingly.[10] Therefore, the glucose analog FDG can be abnormally concentrated in high metabolic sites and malignant tumor tissues, so that FDG tumor imaging has a higher signal-to-noise ratio (SNR) and lesion contrast.[9,10,12] Thus, FDG is recommended to be combined in MET imaging to improve the accuracy of glioma classification.[9,13,14] In another example, PET/CT may be useful for detecting tumors in patients with ambiguous MRI results. When FDG PET/CT produces negative results, MET PET/CT can provide valuable diagnostic information, particularly in patients with recurrent microadenomas.[15] Moreover, FDG and ^{11}C-raclopride have potential applications in the differential diagnosis of Parkinson's disease, progressive supranuclear palsy, and multiple system atrophy.[16,17]

However, due to various factors, such as low injected dose or low specific uptake, some of the radiotracers used under the influence of these factors can yield high noise and low counts images.[16] To solve this problem, some researchers have explored dual-tracer imaging. As reported in the literature, Cheng et al. developed a direct parametric image reconstruction method for estimating kinetic parameters and recovering single-tracer information from rapid multi-tracer PET measurements.[18] Gao et al. suggested a simultaneous dynamic dual-tracer reconstruction of tissue activity maps based on guidance from tracer kinetics.[19] Ellis et al. proposed to use a weighted quadratic maximum a posteriori (MAP) method to reduce the noise of poorer-quality PET images under the guidance of higher-quality datasets.[16,20] In recent studies,[21] some researchers have also compared the MAP approach with the kernel method[22-27] that has recently become popular. The comparison showed that for low-count simulated datasets, the MAP-related method performed poorly due to the inclusion of noisy PET information in the regularization term. In contrast, the kernel-related approach exhibited better performance in terms of achieving the best tradeoff for the reconstruction of the whole brain and PET-unique regions. Thus, taking the characteristics of dual-tracer imaging into account, this paper proposes to introduce higher-quality FDG datasets to guide lower-count MET images by the kernel method. Previously, researchers mainly used the MR prior data in the kernel method to guide PET reconstruction.[25,28,29] This is the first time that another radiotracer image has been adopted to guide the reconstruction of PET images. Various studies comparing MET and FDG have demonstrated that MET is characterized by better sensitivity, specificity, and diagnostic accuracy in detecting, delineating, and finding recurrences of brain tumors.[30] It has also been shown that the combination of FDG and MET information results in the highest prognostic accuracy.[31] MET images are usually noisy due to the short half-life of ^{11}C, so that the diagnostic accuracy is affected. If the proposed method performs well, it may be beneficial to perform both MET and FDG (or other ^{18}F labeled biomarker) scans on the same patients to significantly improve the diagnostic accuracy. We conducted simulation experiments to verify that the proposed method provided good results in denoising and maintaining tumor edge integrity and contrast.

The remaining sections of this paper are organized as follows. Section 2 introduces the kernel method and the proposed algorithm in detail, as well as the design and evaluation metrics of the simulation experiments. Section 3 presents the results of the simulation study. Section 4 discusses various aspects of the research and conclusions are drawn in Section 5.

2 | MATERIALS AND METHODS

2.1 | Problem formulation

PET sinogram data y can be modeled as a set of independent Poisson random variables. The measurement data y have an expectation $\overline{y}$ that is related to the unknown emission image x through the following affine transform:

$$\overline{y} = Px + r, \tag{1}$$

where P is the system matrix and r is a vector containing the random and scattered events. Based on the independent Poisson model, the log-likelihood function L can be given by

$$L(y|x) = \sum_{i=1}^{M} y_i log_{\overline{y}_i}^{-} - \overline{y}_i, \tag{2}$$

where M represents the total number of lines of response.

Inspired by the kernel method for tomographic image reconstruction developed by Wang and Qi,[27] prior information is incorporated through the use of a kernel trick. The PET image x is denoted by a linear function of transformed prior features in a high-dimensional space. This linear function can be found by evaluating a kernel function $k(f_j, f_l)$ for each pair of prior information images at pixels j and l, where f_j and f_l are the feature vectors of prior information for pixels j and l, respectively. The PET image at the j th pixel can be written as

$$x_j = \sum_l \alpha_l k(f_j, f_l). \tag{3}$$

Generally, the pixel intensity values of each feature vector are extracted from the higher-resolution prior image. The vector α is represented as the coefficient image. In this work, a typical choice of the kernel function k named the radial Gaussian kernel is given by

$$k(f_j, f_l) = exp\left(-\frac{\|f_j - f_l\|^2}{2\sigma^2}\right), \tag{4}$$

where σ is a free kernel parameter controlling edge sensitivity. The above kernel representation in an equivalent matrix-vector form is

$$x = K\alpha, \tag{5}$$

where the (j, l)th element of the kernel matrix K is $k(f_j, f_l)$. A full kernel matrix K is usually too large to be directly viewed as a set of basic functions for prior image representation in practice. In this work, the k-nearest neighbor (kNN) method is adopted to construct a sparse matrix; this approach is widely used for graph construction in machine learning.[27,32] The kNN method searches k neighbors for each pixel; in our experiments, k is 20 and is searched in a 7*7 search window, and then the (j, l)th element of the kernel matrix K is determined by the equation

$$K_{jl} = \begin{cases} k(f_j, f_l), f_l \in kNN of f_j, \\ 0, otherwise. \end{cases} \tag{6}$$

where the kNN search is based on the Euclidean distance between f_j and f_l. To easily choose a kernel parameter, the feature points $\{f_j\}$ should be first normalized using

$$\overline{f_{j,l}} = \frac{f_{j,l}}{\sigma_l(f)}, \tag{7}$$

where $\sigma_l(f)$ is the standard deviation of the lth element of f_j over all of the pixels. Moreover, to ensure that the kernel transformation preserves counts, K is normalized through

$$\overline{K} = diag^{-1}[K1_N] K, \tag{8}$$

where 1_N is a vector of length N with all elements being 1.

Substituting the kernel-based image model (5) and normalized matrix $\overline{K}$ into the PET forward model (1), the following kernelized forward projection model is obtained:

$$\overline{y} = P\overline{K}\alpha + r. \tag{9}$$

Then, the optimization problem for PET image reconstruction is found by

$$\hat{\alpha} = arg\max_{\alpha \geq 0} L(y|\overline{K}\alpha), \tag{10}$$

and the well-known expectation-maximization (EM) algorithm can be derived to find the solution by the following update equation:

$$\alpha^{n+1} = \frac{\alpha^n}{\overline{K}^T P^T 1_M}\left(\overline{K}^T P^T \frac{y}{P\overline{K}\alpha^n + r}\right), \tag{11}$$

where 1_M is a vector of length M with each element being 1, the superscript "T" represents matrix transpose, and n is the number of iterations. The vector multiplication and division are both element-wise operations. Once the coefficient image estimate $\hat{\alpha}$ is obtained, the final image estimate $\hat{x}$ is calculated by

$$\hat{x} = \overline{K}\hat{\alpha}. \tag{12}$$

2.2 | Proposed method

Many existing works on prior information-guided PET image reconstruction have focused on using anatomical priors to improve the quality of reconstructed images. The superior contrast of and the resolution provided by prior images were utilized to better define subject-specific information. Here, we present an overlooked alternative method to the use of the same imaging modality of the previous PET image as a prior. More specifically, we incorporate a higher-quality PET (e.g., FDG) image to guide the reconstruction of another lower-quality PET (e.g., MET) dataset to help compensate for the reduced image quality; this can be accomplished by the kernel method mentioned in the previous section, and the overall framework is shown in Figure 1.

For comparison, two types of feature vectors are defined. Higher-quality PET data (FDG) are used to form the feature vectors f_j^{FDG} based on the equation

$$f_j^{FDG} = \left\{ \left(x^{FDG} \right)_j \right\}, \tag{13}$$

where $\left(x^{FDG} \right)_j$ is a local patch[33] centered at voxel j from the FDG image. Hereinafter, this FDG guided reconstruction method is referred to as the FDG-guided KEM method. The second type of feature vector is extracted from a co-registered MR image, as defined by the equation

$$f_j^{MR} = \left\{ \left(x^{MR} \right)_j \right\}, \tag{14}$$

where $\left(x^{MR} \right)_j$ is a local patch based on voxel j in the MR image. This method is referred to as the MR-guided KEM method. In this work, a $7 * 7$ local patch is extracted for each voxel to assemble the feature vectors. Prior to feature extraction, the FDG image and MR image are normalized to ensure that the standard variation of the image inside the brain region is 1, and we set $\sigma = 1$ in equation (4).

As shown in previous publications,[22,28] the MR-guided KEM method could preserve sharp boundaries of PET images. However, it also introduced bias when the PET tracer uptake did not share the same boundary with the prior MR data. Moreover, FDG-guided KEM resulted in
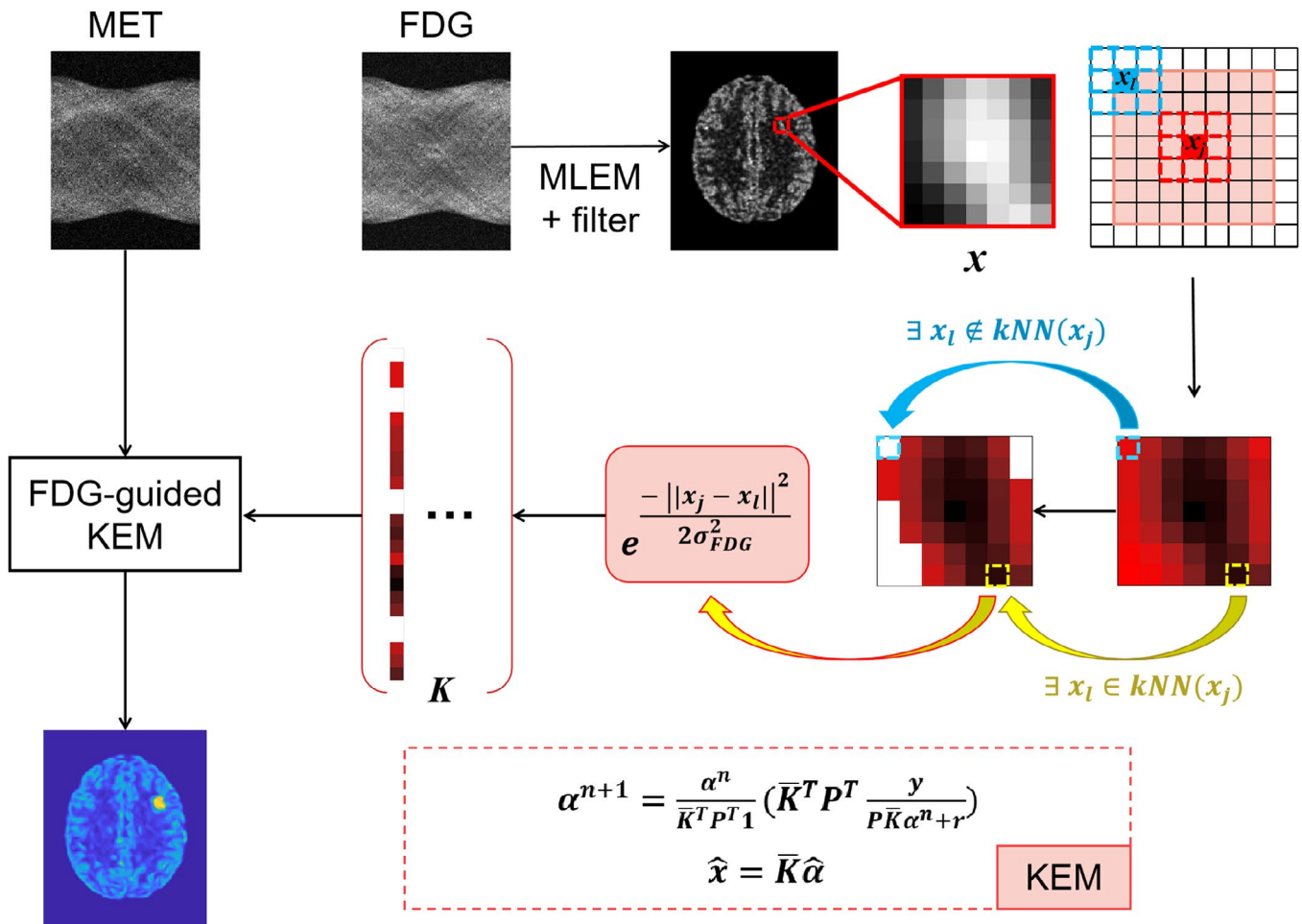
FIGURE 1 The overall framework of dual-tracer PET imaging using the kernel method [Color figure can be viewed at wileyonlinelibrary.com]

higher quality tumor images than MR-guided KEM was found in our simulation. A natural idea is to combine the two types of kernels so that they can compensate for each other while incorporating anatomical information and higher-quality PET data. The intuitive approach is to average the weights of MR and PET features. However, according to the work of Gong and Qi,[24] the structural similarity (SSIM) index is more suitable for finding an appropriate similarity measure and performs well to determine the weights. Thus, this paper adopts the SSIM index to weight the two kinds of features, and the method is referred to as the multi-guided-S KEM method.

2.3 | Experiments and evaluation

To validate the performance of guiding a lower-quality PET (MET) image reconstruction with a higher-quality PET (FDG) image, we simulated two PET emission images and an MR image. The images reconstructed with various methods were compared through visual assessment and quantitative comparisons. Data simulation and image reconstruction were implemented in MATLAB using the MRI data obtained from the BrainWeb project[34] with 217 × 181 voxels in the axial plane and a 1 mm isotropic voxel size.

To generate simulated PET images, a suitable axial slice of the MRI data displaying regions of gray and white matter was chosen for synthesis in a 4:1 ratio, and random noise was added to the corresponding area to make it more realistic. In addition, irregular and uneven lesions were introduced into ground truth PET images between white and gray matter, and the structural boundaries of the lesions of the two PET images were not consistent, as shown in Figure 2. The tumor was hypointense with an intensity that was 60% of that of adjacent white matter in the FDG image, whereas the tumor was hyperintense with a tumor-to-gray matter ratio of 2:1 in the MET image.[16] This distinction simulates the clinically different uptake patterns of the two PET images for tumors.[35,36] Moreover, the enlarged views of the two PET images in Figure 2 show that there

are some brighter areas in the middle of the tumor area of the two PET images for simulating the nonuniformity of the real clinical lesions.[35,37] Based on the general knowledge of clinicians, disease lesions are more easily visible in T2-weighted images than in T1-weighted images. As prior information for MET image reconstruction, a T2-weighted MR phantom was selected from the BrainWeb project and matched with the MET PET image. The T2-weighted image downloaded from the BrainWeb project was lesion-free, and then a lesion was designed in the T2-weighted image with the same shape and the same location as in the MET image and its intensity was taken to be half of the intensity of its surrounding tissue.[26] A CT image obtained from the anatomical classes of the MR image was used as the attenuation map during the reconstruction process, which was derived from Aubert-Broche.[38] The color bar associated with each image shows the intensity of the presented images.[39] Regarding the color bar, the bright color indicates higher intensity and the dark color indicates lower intensity in arbitrary units.

For the simulation study, a GE Discovery ST PET/CT scanner in two-dimensional mode[26,40] was used for the PET image reconstruction. Both the FDG and MET PET phantom images were forward-projected using the system matrix in order to generate noise-free sinograms and independent Poisson noise was introduced into the projection data. In the experiments, the FDG dataset contained 1000 K coincidence events with a 30% uniform background to simulate random and scatter events, whereas the MET dataset contained 500 K coincidence events with a 25% uniform background.[16] To generate the prior image used for guiding the reconstruction of the MET image, the FDG dataset was reconstructed using 100 iterations of MLEM and smoothed by a Gaussian filter with a 4 × 4 kernel.

For the quantitative evaluation of reconstructed results, the image SNR, contrast recovery coefficient (CRC), standard deviation (SD), and mean absolute error (MAE) have often been used as assessment metrics for the reconstruction of PET images. The SNR and SD were defined as
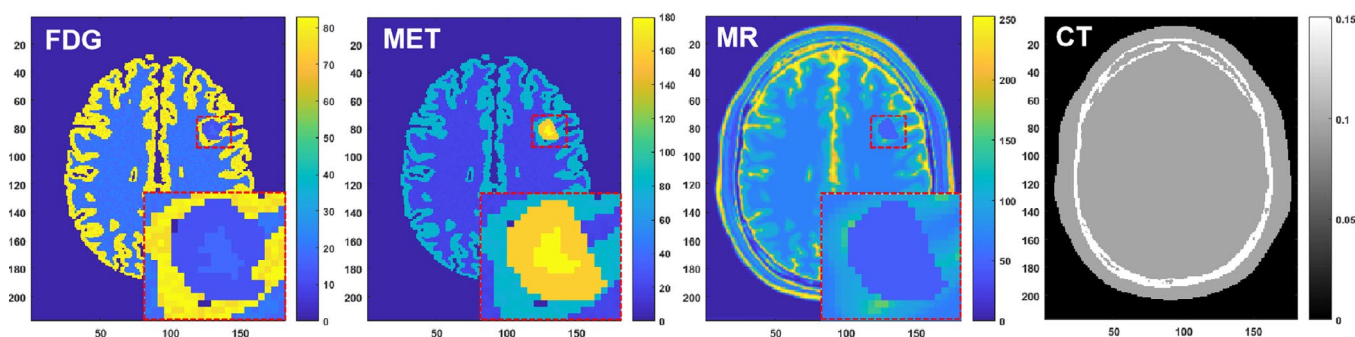
FIGURE 2 Simulated high-resolution ground truth images [Color figure can be viewed at wileyonlinelibrary.com]

$$\text{SNR} = 10\log_{10}\left(\frac{\|x_{\text{recon}}\|^2}{\|x_{\text{recon}} - x_{\text{true}}\|^2}\right), \quad (15)$$

$$\text{SD} = \left(\frac{1}{\overline{x}^{\text{true}}}\sqrt{\frac{1}{n-1}\sum_{j=1}^{n}\left(\overline{x}^j - \overline{x}^{\text{avg}}\right)^2}\right), \quad (16)$$

where $\|\,\|$ represents the Euclidean norm and x_{recon} and x_{true} denote the reconstructed image and ground truth image, respectively. $\overline{x}^j$ represents the mean intensity of the j th realization, and $\overline{x}^{\text{avg}}$ is the average over all noisy realizations. n is the total number of realizations and is set to 20 in this work. In addition, for the j th realization, the CRC was measured through

$$\text{CRC}^j = \left(\frac{\overline{x}^j_{\text{ROI}}}{\overline{x}^j_{\text{BGD}}} - 1\right)\Big/\left(\frac{\overline{x}^{\text{true}}_{\text{ROI}}}{\overline{x}^{\text{true}}_{\text{BGD}}} - 1\right), \quad (17)$$

where $\overline{x}^j_{\text{BGD}}$ is the mean intensity of the background and $\overline{x}^{\text{true}}_{\text{ROI}}$ is calculated from the true background. The CRC was averaged over the realizations and was plotted against its background SD to obtain a CRC versus SD curve. To quantify the reconstruction error, the MAE metric was used that was calculated by

$$\text{MAE} = \frac{100\%}{N_\Phi}\sum_{i \in \Phi}\frac{|x_{i,\text{recon}} - x_{i,\text{true}}|}{x_{i,\text{true}}}, \quad (18)$$

where Φ is the measured region and N_Φ is the total number of voxels in region Φ. For the simulation study, the MAE was used to calculate the whole-brain region and the tumor alone in the MET image.

To compare the FDG-guided KEM for MET image reconstruction, the same datasets were also reconstructed with 100 iterations of conventional MLEM implemented with post-reconstruction denoising methods[27] (Gaussian[16] and NLM[41]), MR-guided KEM and multi-guided-S KEM reconstruction methods. In addition, it is valuable to simulate a range of count levels to investigate the effect of the FDG count level on the kernel reconstruction of the MET data. Moreover, validation of the performance of the proposed reconstruction method is important in the cases of disagreement between the guiding image FDG/MR and the MET image. Therefore, we simulated different counts of FDG and generated mismatched FDG and MR priors. The range of FDG count level is set to 500–1000 K. The mismatched FDG and MR priors were produced by rotating the normal FDG and MR images by 3, 6, and 9° clockwise to simulate the patients' body movements with different amplitudes in the clinic. Other experimental settings were the same as described above.

3 | RESULTS

To assess the performance of the proposed FDG-guided KEM method, comparative experiments were performed using several other algorithms, including MLEM implemented with post-reconstruction denoising methods (Gaussian and NLM), MR-guided KEM, and multi-guided-S KEM. Figure 3 shows the reconstructed images for all of the algorithms and their whole image SNRs; moreover, it also contains enlarged views of the details around the tumor and the SNR of the corresponding position of the tumor. MLEM with smoothing by Gaussian filters achieved a certain level of tumor recognition in the brain image but still exhibited a certain amount of noise and a blurred tumor edge. MLEM followed by NLM denoising yielded great improvement in the SNR of the tumor and the whole image but failed to delineate the tumor boundary. The MR-guided KEM
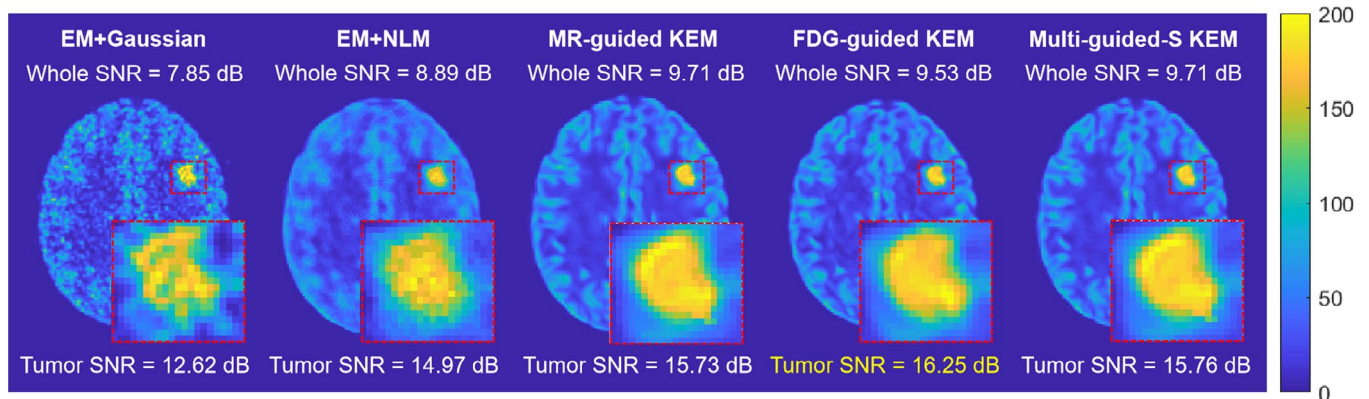

FIGURE 3 Examples of reconstructed images for different algorithms and their whole image SNRs and corresponding tumor SNRs. The FDG-guided KEM method clearly outperformed the MLEM method with smoothing by Gaussian and NLM filters in terms of noise reduction and brain edge preservation while preserving more tumor pathological information than the MR-guided KEM and multi-guided-S KEM, thus yielding the highest tumor SNR of all of the evaluated methods [Color figure can be viewed at wileyonlinelibrary.com]

image and multi-guided-S KEM image were similar in their excellent denoising ability and detail retention. They both yielded the highest whole image SNR, which resulted mainly from the T2-weighted image used for the MR phantom in this work, with an added tumor shape of the same size and at the same position as in the MET phantom. In general, owing to the different imaging patterns, the T2-weighted MRI tumor image would not have the same boundaries as the MET PET image. However, the proposed FDG-guided KEM image still outperformed the multi-guided-S KEM method by 3.11% in the tumor SNR and was better than the Gaussian smoothed MLEM method by 28.76%. The proposed method was superior to the MR-guided KEM method because another tracer (FDG) PET was introduced in the reconstruction process as a prior image to supplement more tumor pathological information, and the supplemented information cannot be derived from the MR prior. The MR-guided reconstruction image could only recover the original tumor information of MET. Therefore, regarding visual representation, as shown in Figure 3, the reconstructed image obtained from the proposed method displayed less noise in the tumor and contained more pathological information than the other reconstructed images.

In addition to visual analysis, some quantitative metrics were chosen to evaluate the reconstruction results of the algorithms. Figure 4a indicates that each of the guided KEM algorithms obtained significantly higher CRCs at the given noise level than the MLEM method with smoothing by Gaussian and NLM filters. Moreover, compared with the MR-guided KEM and multi-guided-S KEM methods, the FDG-guided KEM method achieved a 0.68% improvement in the CRC, but it also slightly increased the background SD. For the MAE metric shown in Figure 4b, both the tumor MAE and whole-brain MAE values of the images obtained from the MLEM method with smoothing by Gaussian and NLM filters were higher than those obtained by the guided KEM methods, which was not a good reconstruction result. The proposed FDG-guided KEM method yielded an 8.07% lower tumor MAE, even though the whole-brain MAE was slightly higher than that of the MR-guided KEM and multi-guided-S KEM methods.

In the kernel method, when extracting features using a patch from the prior image, the neighborhood size is a useful parameter worth exploring. Correspondingly, the kNN search number is important as well. The tradeoff between tumor SD and tumor mean is plotted for different neighborhood sizes and the selected search numbers. As shown in Figure 5, when the neighborhood size was smaller, such as 3 or 5, the MR-guided KEM and multi-guided-S KEM images exhibited the highest means with the smallest SDs among all of the methods. Because there was less structural detail of the FDG image under the smaller neighborhood, the MR prior had a better and more accurate tumor morphology. In
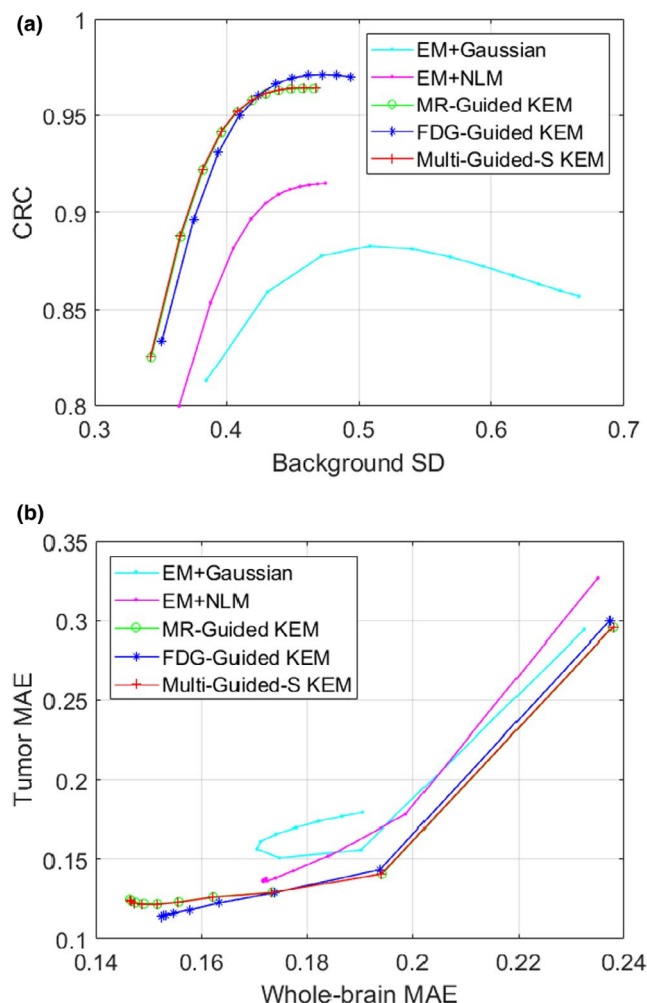
FIGURE 4 Quantitative analysis and comparison of reconstructed images. (a) CRC-background SD tradeoff curve for all of the algorithms. (b) Tumor MAE versus whole-brain MAE curves. The panels show that the CRC and tumor MAE obtained using the FDG-guided KEM method are better than those obtained using the other algorithms [Color figure can be viewed at wileyonlinelibrary.com]

addition, when the neighborhood size was larger, the proposed FDG-guided KEM method exhibited excellent tumor recovery performance. When searching for the 20 nearest neighbors in the 9 × 9 neighborhood, the mean and SD of tumor obtained by the proposed method were significantly better than those of the other comparison methods. Furthermore, among the four neighborhood sizes, searching 20 nearest neighbors in a 7 × 7 neighborhood was the best choice because each method could produce a higher tumor mean while maintaining a lower SD. Therefore, other experiments in this work were based on this choice of parameters.

Generally, an increase in the mean value of the tumor may also increase the SD, as was verified in various KEM methods with smaller neighborhood sizes and MLEM with smoothing by Gaussian filter methods. However, when the neighborhood size became larger, the kernel matrices obtained by the KEM methods
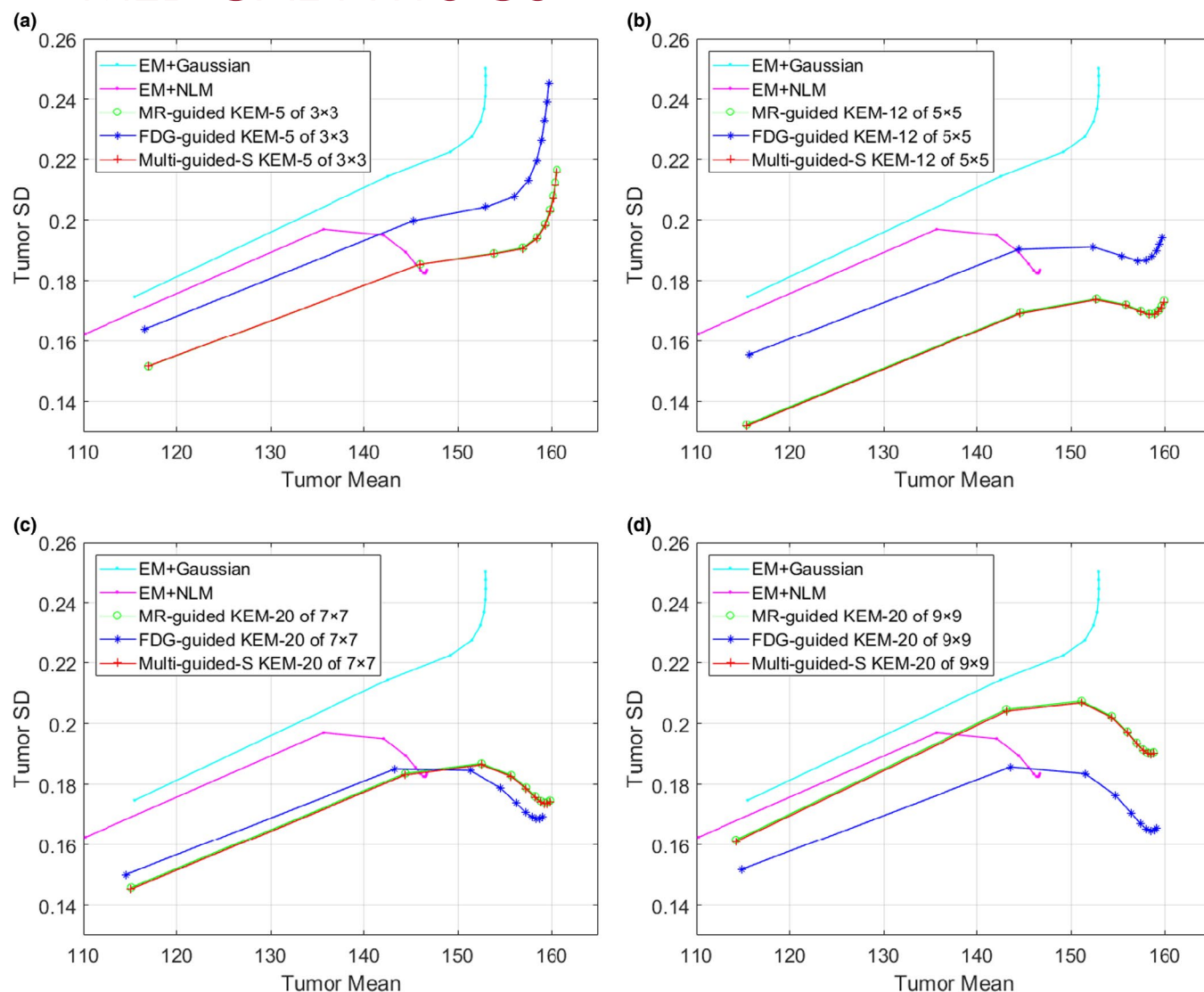
FIGURE 5 Tumor mean-SD tradeoff curve for different neighborhood sizes and the selected search number. The FDG-guided KEM method exhibited a better mean-SD tumor performance than the remaining methods when the neighborhood size was larger. (a) A search for the 5 nearest neighbors in a 3 × 3 neighborhood. (b) A search for the 12 nearest neighbors in a 5 × 5 neighborhood. (c) A search for the 20 nearest neighbors in a 7 × 7 neighborhood. (d) A search for the 20 nearest neighbors in a 9 × 9 neighborhood [Color figure can be viewed at wileyonlinelibrary.com]

contained more detail, so that they could be updated with more accurate tumor information at each iteration. Therefore, the mean value increased while the SD decreased, eventually reaching a steady value. Regarding the MLEM with the NLM filtering method, a lower SD was obtained when the weight value of each pixel was added to the calculation. This guaranteed that when the adjacent and larger difference points were averaged in the neighborhood, their mutual influence was reduced. Thus, the NLM-smoothed MLEM method retained more details of the tumor, and its SD was still lower.

Figure 6 shows the results of the investigation on the effect of the FDG count level on the reconstruction of the MET image. As the count level increased, the results obtained by the FDG-guided KEM method clearly improved, showing more complete tumor boundaries,

and the corresponding SNR gradually increased as well.

To validate the performance of the proposed algorithm when a patient moves unintentionally in the clinic, mismatch experiments between FDG/MR and MET images were considered in our simulation. As observed in the reconstructed images shown in Figure 7, the FDG-guided KEM method could maintain sharper tumor boundaries than the boundaries determined by the MR-guided KEM method when the prior image was rotated. In addition, with respect to the SNR value of the tumor, FDG mismatch and MR mismatch are similarly affected by the rotated prior image. The SNR of the FDG-guided KEM method was reduced by 9.4% (from 16.25 to 14.73 dB), whereas that of the MR-guided KEM method decreased by 9.5% (from 15.73 to 14.23 dB).

FIGURE 6 Investigation of the effect of FDG count level on the performance of the proposed method. The count levels of FDG prior are 500, 750, and 1000 K, respectively. The next row of FDG priors is their corresponding reconstructed images and magnified views of the tumor, with the SNR values given below the images [Color figure can be viewed at wileyonlinelibrary.com]
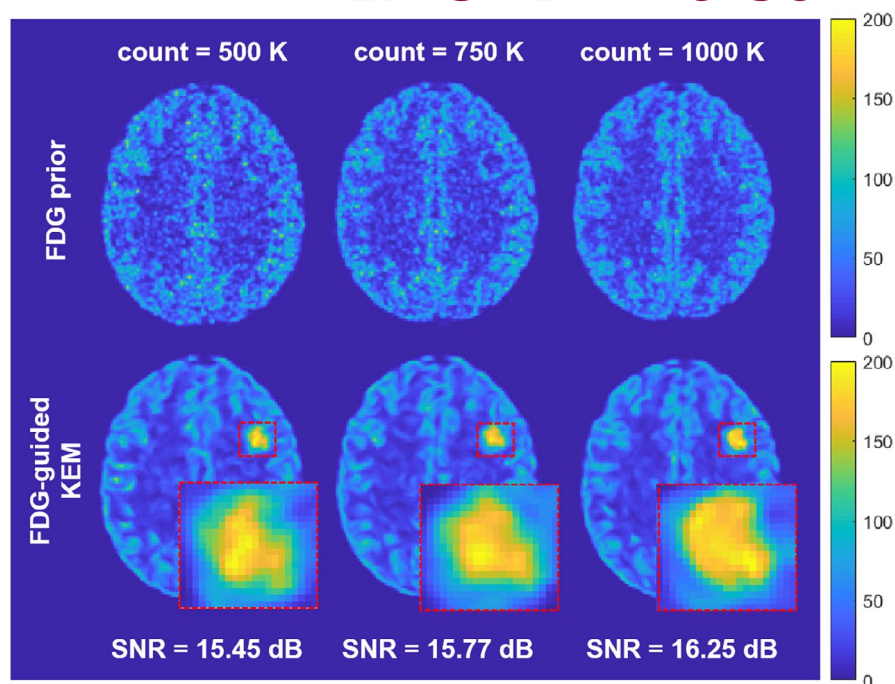
However, from the perspective of the reconstructed tumor morphology, when the rotation angle is smaller, such as 3 or 6°, the tumor boundary of the FDG-guided KEM image is still more clear and more complete than that of the MR-guided KEM image after rotation.

4 | DISCUSSION

In this work, we proposed dual-tracer PET imaging using the kernel method. To validate the performance of the methodology, a simulation study was performed to explore FDG-guided KEM reconstruction and to compare reconstructed images with those of MLEM with smoothing by Gaussian and NLM filters, MR-guided KEM, and multi-guided-S KEM methods. In addition to visual comparison, we quantitatively assessed the proposed FDG-guided KEM method by some metrics and varying individual parameters, particularly for the investigation of the influence of the FDG count level on the reconstructed MET image. Moreover, due to the use of prior information to guide MET data reconstruction, related experiments on the mismatch between the prior FDG/MR and MET were conducted in our simulation. The results of the present experiments suggested that the proposed FDG-guided KEM method outperformed the other algorithms.

Many existing works on prior information to guide PET imaging have focused mainly on utilizing anatomical images (e.g., MR). Many MR imaging techniques, such as T1-weighted imaging, T2-weighted imaging, dynamic contrast enhancement (DCE) imaging, and diffusion-weighted imaging (DWI), are currently available. Among them, the T1-weighted image was

frequently used as a prior image for PET reconstruction because it yielded rich structural information[22,24,28]; by contrast, T2-weighted, DCE or DWI images exhibited enhanced lesion information, rendering the tumor more visible. Since this work proposed to use another tracer PET for guided reconstruction, the functional lesion information of the prior image was more dominant. Thereby, a T2-weighted image that contained more lesion information was selected to be an MR prior image in this work.

For the simulated MR prior, a tumor was added into the T2-weighted image of the same shape and same location as the MET image, which was more conducive for MR prior to guide MET image reconstruction. In general, different imaging techniques reflect various characteristics of the tumor, so the T2-weighted MRI tumor image would not have the same boundaries as either the FDG or MET PET images. The implementation as described in this work may not be the case in the clinic, which limits the accuracy of the simulation experiments in the study.

The advantage of PET lies in the rich tissue metabolism information that cannot be derived from the MR images. Therefore, the same imaging modality of the PET image to be reconstructed but using a different radiotracer image is proposed as a prior. As described in this paper, the proposed FDG-guided KEM method can better compensate with tumor metabolism information of the image to be reconstructed than the other methods. Even though the MR-guided image had excellent tumor delineation and there was less noise in the image, it still only recovered the tumor information of the original MET and could not supplement the tumor information of another tracer FDG. In addition, from a clinical perspective, metabolic
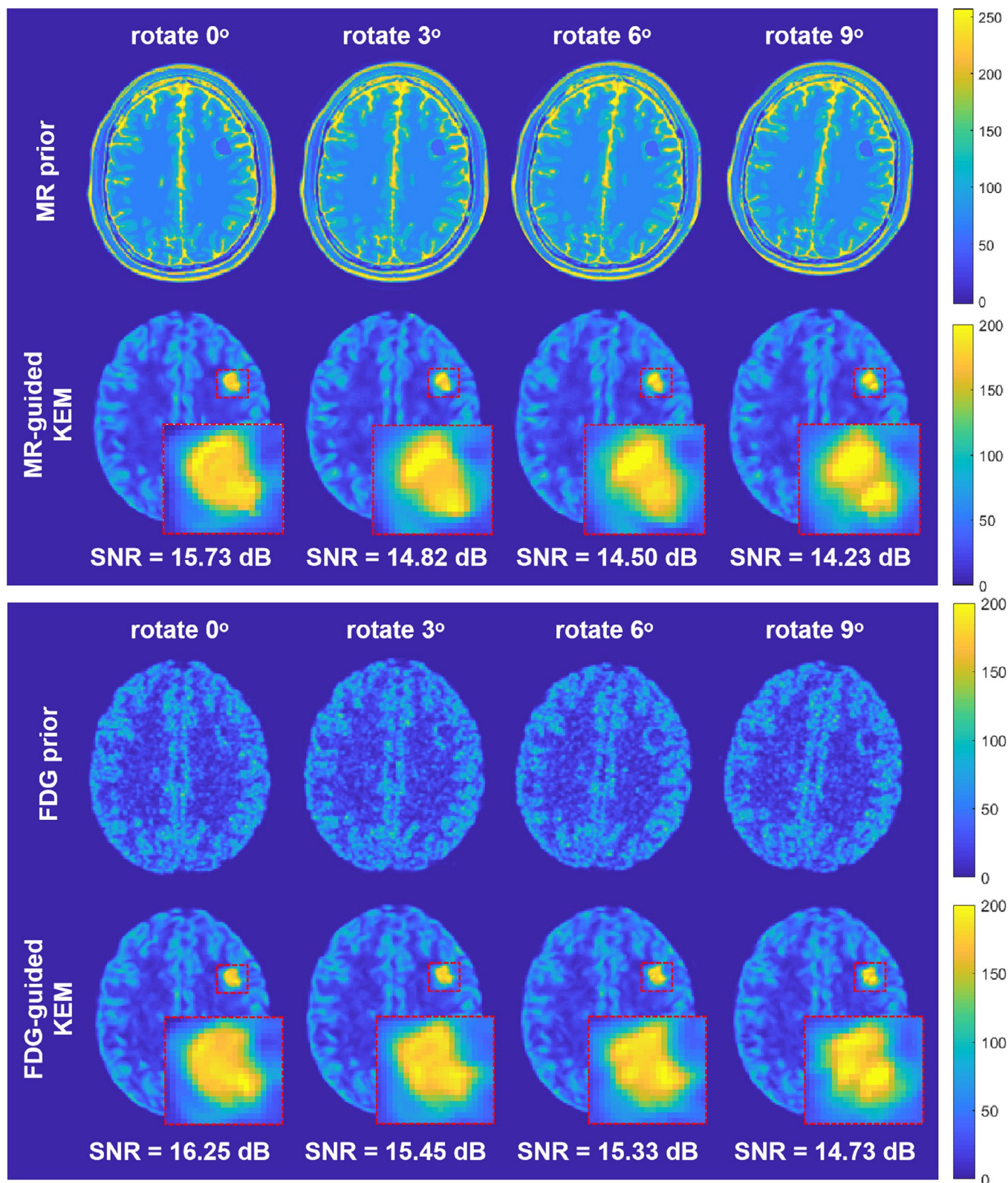
FIGURE 7 Mismatched FDG/MR priors and example reconstruction images from the mismatch experiments. Both the MR and FDG priors are rotated clockwise by 0, 3, 6, and 9°, respectively. The next row of the prior images is their corresponding reconstructed images and enlarged views of the tumor, with the SNR values attached below the images [Color figure can be viewed at wileyonlinelibrary.com]

information supplemented by FDG images may also be beneficial for diagnosis and disease stage identification. Furthermore, as shown in Figures 3 and 4, the proposed FDG-guided KEM method yielded the highest SNR and CRC of the tumor region compared with those derived from the other algorithms. Undoubtedly,

the distribution of the tumor may also be incorrectly supplemented, depending on the specific uptake intensity of the tumor to the radiotracer. Thus, future work can perform more specific dual tracer reconstruction in this field. Clinically, more different kinds of tracers will be combined according to the actual case situation. The FDG-guided MET reconstruction imaging in this work is just one example of this approach. In future work, it can be combined with specific diseases for more in-depth research. From the perspective of the reconstruction algorithm, currently, there is another dual-tracer reconstruction imaging approach using MAPEM, as mentioned in the introduction, but the comparison of the two dual-tracer reconstruction methods was not the focus of this paper and can be considered in future research. This paper mainly focused on using an existing popular kernel algorithm in practical dual-tracer imaging.

By altering various parameters in the kernel method, including the neighborhood size and the search number of kNN, more suitable parameter values of the proposed method and other comparison algorithms were selected. In our simulation experiments, four kinds of neighborhoods and the corresponding search numbers were chosen, as shown in Figure 5. According to the results, searching 20 nearest neighbors in a 7 × 7 neighborhood was the optimal choice for the guided KEM method. Therefore, for the trend indicating the optimization of the two parameters, the promotion effect was limited; that is, searching the 20 nearest neighbors in a 7 × 7 neighborhood for each voxel to extract kernel features was used to build an adequately similar kernel matrix to guide the reconstruction.

The investigation results shown in Figure 6 have certain practical significance with regard to the influence of the FDG count level on MET image reconstruction. Although a higher count level of the guided image can obtain a higher quality of image reconstruction, the count level is still limited to the actual clinical situation, such as the patient's drug tolerance. Therefore, guide images with different count levels can be selected for image reconstruction according to the conditions of different patients in the clinic.

When guiding PET image reconstruction using the prior, the mismatch problem inevitably needs to be considered. As shown in Figure 7, mismatch experiments were performed between FDG/MR and MET data. In the simulation study in this paper, although some uneven and inconsistent operations were performed for ground truth images (Figure 2), they still have similar anatomical structures that may have provided unfair benefits to the guided KEM method because of the close correspondence between the prior and the image to be reconstructed. However, the effect on noise removal and detail preservation for the reconstructed image using the guided KEM algorithms was undeniable, so that in both the mismatch FDG-MET and MR-MET

experiments, the features of the tumors were sharper in the guided KEM image reconstruction than those in the Gaussian and NLM smoothed MLEM reconstruction. However, when rotated to 9°, the tumor SNR of the FDG/MR-guided image was significantly decreased. Therefore, when a similar larger mismatch occurs, FDG/MR guidance should be reconsidered clinically to prevent the weakening of MET metabolism information. To the best of our knowledge, many excellent rigid body registration tools are available for correcting misregistration for images of the brain, such as Advanced Normalization Tools (ANTS), Elastix, and NiftyReg.[42] Among the registration tools, ANTS achieved better registration accuracy, while Elastix possessed higher computational efficiency with acceptable accuracy.[42] In addition, with the development of PET/MR scanners and dual-tracer PET protocols, the mismatch problem is being resolved.

MR image and FDG data can be combined as multimodality prior to MET reconstruction. In this work, the SSIM index was used to find an appropriate similarity measure to determine the weight between the two modalities of information. Unfortunately, according to the experimental results, the performance of multi-guided-S KEM was similar to that of MR-guided KEM; this may be mainly because the SSIM index is based on structural similarity. In other words, the similarity measure ρ should be high (close to 1) in the regions where the FDG and MR images share the same boundary and it should be low (close to 0) in the regions where their boundaries do not match.[24] This made the weights of the two priors biased toward the MR images with good structural information; thus, the multi-guided-S KEM could not outperform the MR-guided KEM but rather achieve similar performance. Weighing the multimodality prior information will need to be explored in future work.

Since the proposed method has been verified only on 2-D simulation data, further verification of the clinical data is still necessary. In future work, parallel GPU calculations can be utilized to further improve the computational efficiency and cooperation with the hospital can be enhanced to acquire real datasets for a more accurate evaluation of the results obtained by the proposed method.

5 | CONCLUSIONS

Based on our simulation study, we demonstrated improved performance of the proposed FDG-guided KEM method compared to other algorithms in terms of the tradeoff between noise reduction of the whole brain and detail preservation of the lesion. This work focuses on combining multiple tracers to improve the accuracy of disease diagnosis and the specificity and sensitivity of tumor characterization. Using the kernel

algorithm, the features of a higher-count PET image are extracted in higher dimensions to guide the reconstruction of the lower-count PET image that can be supplemented based on the original tumor distribution and may also have certain clinical application significance for the diagnosis and staging of diseases. Through various experiments, it was shown that compared with other algorithms, the proposed algorithm demonstrated significantly better performance in providing pathological information regarding tumor maintenance. In summary, the proposed FDG-guided KEM method can effectively utilize and compensate for the tissue metabolism information obtained from dual-tracer PET to maximize the advantages of PET imaging.

CONFLICT OF INTEREST
The authors have no conflicts to disclose.

DATA AVAILABILITY STATEMENT
The data that support the findings of this study are available in the Normal Brain Database at https://brainweb.bic.mni.mcgill.ca/.

REFERENCES

1. Hu Z, Xue H, Zhang Q, et al. DPIR-Net: direct PET image reconstruction based on the Wasserstein generative adversarial network. *IEEE Trans Radiat Plasma Med Sci*. 2021;5(1):35-43. http://doi.org/10.1109/trpms.2020.2995717
2. Hu Z, Li Y, Zou S, et al. Obtaining PET/CT images from non-attenuation corrected PET images in a single PET system using Wasserstein generative adversarial networks. *Phys Med Biol*. 2020;65:215010.
3. Zhang Q, Gao J, Ge Y, et al. PET image reconstruction using a cascading back-projection neural network. *IEEE J Sel Top Signal Process*. 2020;14(6):1100-1111. http://doi.org/10.1109/jstsp.2020.2998607
4. Zeng T, Gao J, Gao D, et al. A GPU-accelerated fully 3D OSEM image reconstruction for a high-resolution small animal PET scanner using dual-ended readout detectors. *Phys Med Biol*. 2020;65:245007.
5. Zhang W, Gao J, Yang Y, et al. Image reconstruction for positron emission tomography based on patch-based regularization and dictionary learning. *Med Phys*. 2019;46:5014-5026.
6. Carter SF, et al. Evidence for astrocytosis in prodromal Alzheimer disease provided by 11C-deuterium-L-deprenyl: a multitracer PET paradigm combining 11C-Pittsburgh compound B and 18F-FDG. *J Nucl Med*. 2012;53:37-46.
7. Chung J-K, Kim Y, Kim S, et al. Usefulness of 11C-methionine PET in the evaluation of brain lesions that are hypo- or isometabolic on 18F-FDG PET. *Eur J Nucl Med Mol Imaging*. 2002;29(2):176-182. http://doi.org/10.1007/s00259-001-0690-4
8. Cook GJ, Maisey MN, Fogelman I. Normal variants, artefacts and interpretative pitfalls in PET imaging with 18-fluoro-2-deoxyglucose and carbon-11 methionine. *Eur J Nucl Med*. 1999;26:1363-1378.
9. Jiang T. Guidelines for diagnosis and treatment of glioma (2018 Edition). *Chin J Neurosurg*. 2019;35:217-241. (in Chinese).
10. Kong Y, Guan Y. Application progress of PET molecular imaging of glioma. *Oncoradiol*. 2016;25:196-208. (in Chinese).
11. Heiss W-D. Clinical impact of amino acid PET in gliomas. *J Nuclear Med*. 2014;55(8):1219-1220.
12. la Fougere C, Suchorska B, Bartenstein P, Kreth F-W, Tonn J-C. Molecular imaging of gliomas with PET: opportunities and limitations. *Neuro-oncol*. 2011;13:806-819.
13. Katsanos AH, Alexiou GA, Fotopoulos AD, et al. Performance of 18F-FDG, 11C-methionine, and 18F-FET PET for glioma grading: a meta-analysis. *Clin Nucl Med*. 2019;44:864-869.
14. Kim YH, Oh SW, Lim YJ, et al. Differentiating radiation necrosis from tumor recurrence in high-grade gliomas: assessing the efficacy of 18F-FDG PET, 11C-methionine PET and perfusion MRI. *Clin Neurol Neurosurg*. 2010;112:758-765.
15. Feng Z, He D, Mao Z, et al. Utility of 11C-methionine and 18F-FDG PET/CT in patients with functioning pituitary adenomas. *Clin Nucl Med*. 2016;41:e130-e134.
16. Ellis S, Mallia A, McGinnity CJ, Cook GJ, Reader AJ. Multitracer guided PET image reconstruction. *IEEE Trans Radiat Plasma Med Sci*. 2018;2:499-509.
17. El Fakhri G, Trott CM, Sitek A, Bonab A, Alpert NM. Dual-tracer PET using generalized factor analysis of dynamic sequences. *Mol Imag Biol*. 2013;15:666-674.
18. Cheng X, Li Z, Liu Z, et al. Direct parametric image reconstruction in reduced parameter space for rapid multi-tracer PET imaging. *IEEE Trans Med Imaging*. 2015;34:1498-1512.
19. Gao F, Liu H, Jian Y, Shi P. Dynamic dual-tracer PET reconstruction. In: Prince JL, Pham DL, Myers KJ, eds. *International Conference on Information Processing in Medical Imaging*. Berlin: Springer; 2009:38-49.
20. Ellis S, Mallia A, McGinnity CJ, Cook GJ, Reader AJ. Guided image reconstruction for multi-tracer PET. In: Aarsvold J, ed. *2017 IEEE Nuclear Science Symposium and Medical Imaging Conference (NSS/MIC)*. New York: IEEE; 2017:1-3.
21. Bland J, Mehranian A, Belzunce MA, et al. Intercomparison of MR-informed PET image reconstruction methods. *Med Phys*. 2019;46:5055-5074.
22. Tahaei MS, Reader AJ, Collins DL. Two novel PET image restoration methods guided by PET-MR kernels: application to brain imaging. *Med Phys*. 2019;46:2085-2102.
23. Wang G. High temporal-resolution dynamic PET image reconstruction using a new spatiotemporal kernel method. *IEEE Trans Med Imaging*. 2019;38(3):664-674. http://doi.org/10.1109/tmi.2018.2869868
24. Gong K, Cheng-Liao J, Wang G, Chen KT, Catana C, Qi J. Direct Patlak reconstruction from dynamic PET data using the kernel method with MRI information based on structural similarity. *IEEE Trans Med Imaging*. 2018;37(4):955-965. http://doi.org/10.1109/tmi.2017.2776324

25. Novosad P, Reader AJ. MR-guided dynamic PET reconstruction with the kernel method and spectral temporal basis functions. *Phys Med Biol.* 2016;61:4624.

26. Hutchcroft W, Wang G, Chen KT, Catana C, Qi J. Anatomically-aided PET reconstruction using the kernel method. *Phys Med Biol.* 2016;61:6668.

27. Wang G, Qi J. PET image reconstruction using kernel method. *IEEE Trans Med Imaging.* 2015;34(1):61-71. http://doi.org/10.1109/tmi.2014.2343916

28. Bland J, Belzunce MA, Ellis S, et al. Spatially compact MR-Guided kernel EM for PET image reconstruction. *IEEE Trans Radiat Plasma Med Sci.* 2018;2:470-482.

29. Ehrhardt MJ, Thielemans K, Pizarro L, et al. Joint reconstruction of PET-MRI by exploiting structural similarity. *Inverse Prob.* 2015;31(1):015001. http://doi.org/10.1088/0266-5611/31/1/015001

30. Glaudemans AWJM, Enting RH, Heesters MAAM, et al. Value of 11C-methionine PET in imaging brain tumours and metastases. *E J Nucl Med Mol Imaging.* 2013;40(4):615-635. http://doi.org/10.1007/s00259-012-2295-5

31. Van Laere K, Ceyssens S, Van Calenbergh F, et al. Direct comparison of 18F-FDG and 11C-methionine PET in suspected recurrence of glioma: sensitivity, inter-observer variability and prognostic value. *E J Nucl Med Mol Imaging.* 2005;32(1):39-51. http://doi.org/10.1007/s00259-004-1564-3

32. Friedman JH, Bentley JL, Finkel RA. An algorithm for finding best matches in logarithmic expected time. *ACM Trans Math Softw.* 1977;3(3):209-226.

33. Tahaei MS, Reader AJ. Patch-based image reconstruction for PET using prior-image derived dictionaries. *Phys Med Biol.* 2016;61:6833.

34. Cocosco CA, Kollokian V, Kwan RK-S, Pike GB, Evans AC. Brainweb: Online interface to a 3D MRI simulated brain database. *NeuroImage.* 1997;5:425.

35. Borbély K, Nyáry I, Tóth M, Ericson K, Gulyás B. Optimization of semi-quantification in metabolic PET studies with 18F-fluorodeoxyglucose and 11C-methionine in the determination of malignancy of gliomas. *J Neurol Sci.* 2006;246:85-94.

36. Pirotte B, et al. Comparison of 18F-FDG and 11C-methionine for PET-guided stereotactic brain biopsy of gliomas. *J Nucl Med.* 2004;45:1293-1298.

37. Takahashi M, Soma T, Mukasa A, et al. Pattern of FDG and MET distribution in high-and low-grade gliomas on PET images. *Clin Nucl Med.* 2019;44:265-271.

38. Aubert-Broche B, Evans AC, Collins L. A new improved version of the realistic digital brain phantom. *NeuroImage.* 2006;32:138-145.

39. Li T, Thorndyke B, Schreibmann E, Yang Y, Xing L. Model-based image reconstruction for four-dimensional PET. *Med Phys.* 2006;33:1288-1298.

40. Mawlawi O, Podoloff DA, Kohlmyer S, et al. Performance characteristics of a newly developed PET/CT scanner using NEMA standards in 2D and 3D modes. *J Nucl Med.* 2004;45:1734-1742.

41. Buades A, Coll B, Morel JM. On image denoising methods. *CMLA Preprint.* 2004;5:19-26.

42. Nazib A, Galloway J, Fookes C, Perrin D. Performance of registration tools on high-resolution 3d brain images. Weiland James, ed. *2018 40th Annual International Conference of the IEEE Engineering in Medicine and Biology Society (EMBC).* New York: IEEE; 2018:566-569.